The P4-ATPase Drs2 regulates homeostasis of Atg9

Irene Pazos[1], Marta Puig-Tintó[1], Jorge Cordero[1], Nereida Jiménez-Menéndez[1], Marc Abella[1,2], Ana G. Duran[1,3], Emi Adachi-Fernández[1], Carla Belmonte-Mateos[1], Susana Sabido-Bozo[4,5], Altair Chinchilla[1], Sébastien Tosi[6], Akiko Nezu[7,8], Julien Colombelli[6], Todd R. Graham[9], Tamotsu Yoshimori[7,8], Manuel Muñiz[4,5], Maho Hamasaki[7,8], Oriol Gallego[1,*]

[1]Department of Experimental and Health Sciences (DCEXS), Pompeu Fabra University (UPF), 08003 Barcelona, Spain.
[2]Present address: Department of Systems and Synthetic Microbiology, Max Planck Institute for Terrestrial Microbiology, 35043 Marburg, Germany.
[3]Present address: Institute of Biomaterial Science, Helmholtz-Zentrum Geesthacht, Kantstr. 55, 14513 Teltow, Germany.
[4]Department of Cell Biology, University of Seville, 41012 Seville, Spain.
[5]Instituto de Biomedicina de Sevilla (IBiS), Hospital Universitario Virgen del Rocío/CSIC/Universidad de Sevilla, 41012 Seville, Spain.
[6]Institute for Research in Biomedicine (IRB Barcelona), The Barcelona Institute of Science and Technology, (BIST), 08028 Barcelona, Spain.
[7]Department of Genetics, Graduate School of Medicine, Osaka University, Osaka 565-0871, Japan.
[8]Department of Intracellular Membrane Dynamics, Graduate School of Frontier Biosciences, Osaka University, Osaka 565-0871, Japan.
[9]Department of Biological Sciences, Vanderbilt University, Nashville, TN, United States.
[*]Correspondence and requests for materials should be addressed to O.G. Email: oriol.gallego@upf.edu

Abstract

Atg9 is a transmembrane protein essential for selective autophagy, a pathway that mediates the targeted degradation of cellular components to sustain the cell fitness. To preserve the functionality of this pathway, the cell adjusts the transport of vesicles loaded with Atg9 through mechanisms that are not understood. Here we used live-cell imaging to investigate the interactome that regulates Multisubunit Tethering Complexes (MTCs), a set of conserved protein complexes that control vesicle tethering. We found that P4-ATPases, a family of lipid transporters involved in the biogenesis of vesicles, interact with MTCs that participate in the transport of Atg9, such as TRAPPIII. Using the lipid flippase Drs2, we demonstrated that the I(S/R)TTK motif nested in the N-terminal tail cavity of P4-ATPases is necessary for the interaction with MTCs and to maintain the homeostasis of Atg9. At low temperature, the cell enhances the assembly of the Drs2-TRAPPIII module and Drs2 is fundamental for the early stages of selective autophagy, a function that is independent from its activity as lipid flippase and its role in other vesicle transport pathways.

Selective autophagy is a catabolic process that targets the degradation of cellular components, such as organelles, protein aggregates or pathogens, in a specific manner. Selective autophagy requires the *de novo* formation of double membrane compartments, generally called autophagosomes, to confine the selected cargo and to deliver it to the vacuole/lysosomes for subsequent processing[1,2,3,4,5,6]. Selective autophagy has a main role in preserving the cell fitness in front of pathogens or stress, but it is also necessary to maintain the cell biology in processes such as endocytosis[7,8]. The Autophagy-related protein 9 (Atg9) is a transmembrane protein that has recently been characterized as a lipid scramblase [9,10], and it is essential for the formation of the double membrane engulfing the cargo. In growing cells, Atg9 localizes at endocytic compartments, the Golgi and numerous cytoplasmic vesicular structures, which move quickly throughout the cytoplasm[11]. When required, a fraction of Atg9 is mobilized to the pre-autophagosomal structure (PAS), where autophagosome biogenesis takes place. Despite the main role of Atg9, the mechanisms regulating Atg9 homeostasis and its trafficking in the endomembrane system remain unclear.

Multisubunit Tethering Complexes (MTCs) are a group of protein complexes essential for vesicle transport, including the trafficking of Atg9 vesicles. MTCs mediate the tethering of the vesicle to the acceptor membrane through long-range interactions that precede vesicle fusion and cargo delivery at the destination of the transport pathway[12]. Eight MTCs have been described in yeast, all conserved in humans[13]. The conserved oligomeric Golgi (COG) complex is a heterooctamer involved in intra-Golgi retrograde transport[14]. Dsl1, with only three different subunits, is responsible for tethering COPI vesicles derived from the Golgi to the endoplasmic reticulum (ER)[15]. The class C core vacuole/endosome tethering (CORVET) complex and the homotypic fusion and vacuole protein sorting (HOPS) complex share a common core of four subunits and they have two additional specific subunits each. Both complexes act at the endosomal/vacuolar pathway where CORVET tethers vesicles at early endosomes and HOPS functions in late endosomes and the vacuole[16].

The Golgi-associated retrograde protein (GARP) complex is a hetero-tetramer that tethers vesicles derived from endosomes to the trans-Golgi network (TGN)[17]. The exocyst is a heterooctamer responsible for tethering secretory vesicles to the plasma membrane[18]. Finally, the transport protein particle (TRAPP) complexes have historically been classified as MTCs despite their major role as guanine nucleotide exchange factors (GEF) for Rab GTPases[19]. TRAPP comes in two flavors: TRAPPII and TRAPPIII[20]. Both complexes share a heterohexamer core called TRAPPI. TRAPPII comprises TRAPPI plus four more specific subunits[21], whereas TRAPPIII involves the common core and the specific subunit Trs85[22]. TRAPPII activates Ypt31/32 to regulate intra-Golgi transport[23]. TRAPPIII activates Ypt1 to regulate the transport of ER-derived COPII vesicles to the Golgi[22]. The work of multitude of groups showed that COG, GARP, TRAPPII and TRAPIII are key in the transport of Atg9[24,25,26,27]. However, studies have been centered on individual MTCs, which limited the understanding of the molecular bases that play a general role in MTC's function.

To shed light on the molecular mechanisms that control vesicle transport, we have systematically determined interactions that are functionally relevant for MTCs. Our approach combines genetic interactions and PICT (Protein interactions from Imaging Complexes after Translocation), a method to detect protein-protein interactions by live-cell imaging[28,29]. We found that MTCs involved in the anterograde and retrograde transport at the Golgi (TRAPPII, TRAPPIII, GARP, and COG) present a similar interaction pattern with Type IV P-type ATPases (P4-ATPases), a family of lipid translocases that maintain membrane asymmetry by accumulating phospholipids to the cytosolic leaflet. We further investigated the functional relevance of these interactions using Drs2, a P4-ATPase located at the TGN and early endosomes that flips phosphatidylserine (PS) specifically[30,31]. Here, we show that Drs2 is necessary for the correct function of TRAPPIII in selective autophagy, a role that is exacerbated at lower temperatures. Drs2 is essential to maintain Atg9 homeostasis through a mechanism that is independent of its known functions. The mode of action of Drs2 requires a motif located in a cavity of its N-terminal tail. This motif is conserved in other flippases and it defines the network of interactions between P4-ATPases and MTCs.

Results

Protein-protein interactions relevant for MTCs' function

In an effort to thoroughly explore the space of protein interactions that are relevant for MTCs function, we conducted a genome-wide search based on reported genetic interactions in yeast[32]. Genes coding for MTCs subunits establish 2587 genetic interactions with 1283 other genes. Based on the probability of these genetic interactions to occur randomly, we selected those gene products that are more likely to be functionally linked with MTCs. Overall, we selected 470 proteins for subsequent protein-protein interaction screening (see Methods).

We then used the PICT assay to screen protein-protein interactions directly in living cells[28,29] (Fig. 1a). PICT is based in the rapamycin-induced heterodimerization of the FK506-binding protein (FKBP) and the FKBP-rapamycin binding (FRB) domain[33,28]. The addition of rapamycin to the media induces the translocation of proteins tagged with FRB (bait-FRB) to intracellular anchoring platforms tagged with FKBP and RFP (anchor-FKBP-RFP). If a GFP-tagged query protein (prey-GFP) interacts with the bait-FRB, it will build-up at the anchor, which can be quantified by the increment in the co-localization of the GFP and RFP signals (see Methods). Recently, we increased PICT sensitivity up to 200-fold by designing a new anchoring platform. Briefly, we engineered yeast cells to express anchoring platforms at the spindle pole body by tagging Tub4 with FKBP and RFP. The resulting cells harbor one or two anchoring platforms only. Thus, even low abundant complexes accumulate enough prey-GFP in each of these anchoring platforms to be efficiently detected and quantified[29].

The screening identified seven proteins, all conserved in humans, which establish eight protein-protein interactions with MTCs (Figs. 1b and c). The COG complex showed binding to Snc2, an exocytic SNARE known to traffic through the Golgi[34]. CORVET interacts with Hse1, Bro1, Vps45 and Vps9, all involved in the sorting of vacuolar proteins. These interactions provide molecular bases to the mechanism that underlies the interplay between CORVET and the Vps9-Vps21-Vps45 module[35,36].

The interactions that caught our attention were Drs2 binding to TRAPPII and TRAPPIII, and Lem3 binding to GARP. Drs2 is one of the five yeast P4-ATPases together with Dnf1, Dnf2, Dnf3 and Neo1. Except for the last, all P4-ATPases act as heterodimers with its ß-subunit: Lem3 for Dnf1 and Dnf2; Cdc50 for Drs2; and Crf1 for Dnf3[37,38]. The interaction between MTCs and P4-ATPases was unexpected given the canonical role of P4-ATPases in early stages of vesicles biogenesis and of MTCs in vesicle tethering at the last steps of vesicle transport. These results prompted us to further investigate the interplay between lipid flippases and MTCs.

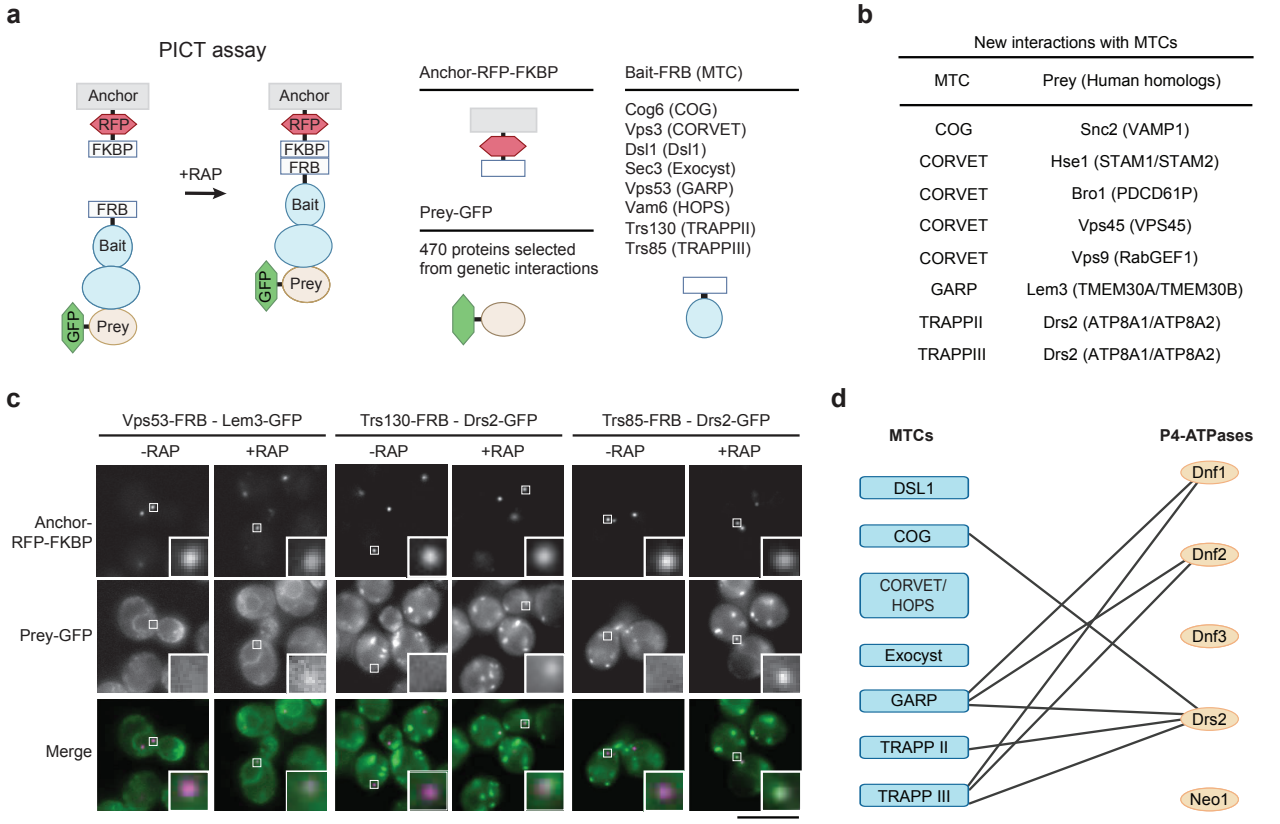

Fig. 1 PICT assay and protein-protein interactions relevant for MTCs' function. **a** Illustration of the PICT assay (left). Most efficient baits used to anchor each MTC (in parenthesis) are listed (top right) (see Supplementary Table 2). **b** Summary of detected protein-protein interactions. Human homologs are indicated in parenthesis. **c** PICT assay for the interactions between indicated pairs of proteins tagged to FRB and GFP. Representative images before and after adding rapamycin (RAP) of RFP-tagged anchor and GFP-tagged prey are shown in the upper and middle row, respectively. Bottom row shows the merged images. White zoom in boxes, 0.9µm. Scale bar, 5µm. **d** Network of interactions between MTCs and P4-ATPases. MTCs are represented by blue boxes and P4-ATPases by orange oval circles. Black lines show the interactions found with PICT.

The network of interactions between MTCs and P4-ATPases

To gain a deeper understanding of the connection between MTCs and P4-ATPases, we expanded the study of protein-protein interactions to all MTCs and P4-ATPases (Fig. 1d). Detected binding events define a network where GARP and TRAPPIII concentrate most of the interactions with P4-ATPases Drs2, Dnf1 and Dnf2. Note that Dnf1 and Dnf2, which show identical binding specificity with MTCs, are also known to have redundant functions[39]. In addition to GARP and the TRAPP complexes, Drs2 also interacts with COG, being the flippase that shows a higher number of interactions with MTCs. These P4-ATPases show preference to bind MTCs involved in trafficking pathways at the Golgi. The binding to COG, GARP, TRAPPII and TRAPPIII might be part of the molecular mechanisms that P4-ATPases use to regulate vesicle trafficking in this organelle. To understand better the molecular mechanism underlying these functions, we further investigated Drs2, the most studied P4-ATPase and the only one whose atomic structure is available[40,41].

Drs2 regulates TRAPPIII function at low temperatures

We first investigated the relevance of Drs2 in TRAPPIII function. TRAPPIII is necessary for the Cytoplasm-to-Vacuole Targeting (CVT) pathway, a model for the study of selective autophagy. The CVT pathway initiates with the construction of the PAS (pre-autophagosomal structure). Then, a double membrane elongates from the PAS to enwrap the precursor Ape1 (prApe1) aminopeptidase until it closes generating the CVT vesicle. TRAPPIII-mediated transport of Atg9 is essential for the biogenesis of the CVT vesicle[27]. After fusion and internalization in the vacuole, prApe1 is processed to mature Ape1 (mApe1)[6,42].

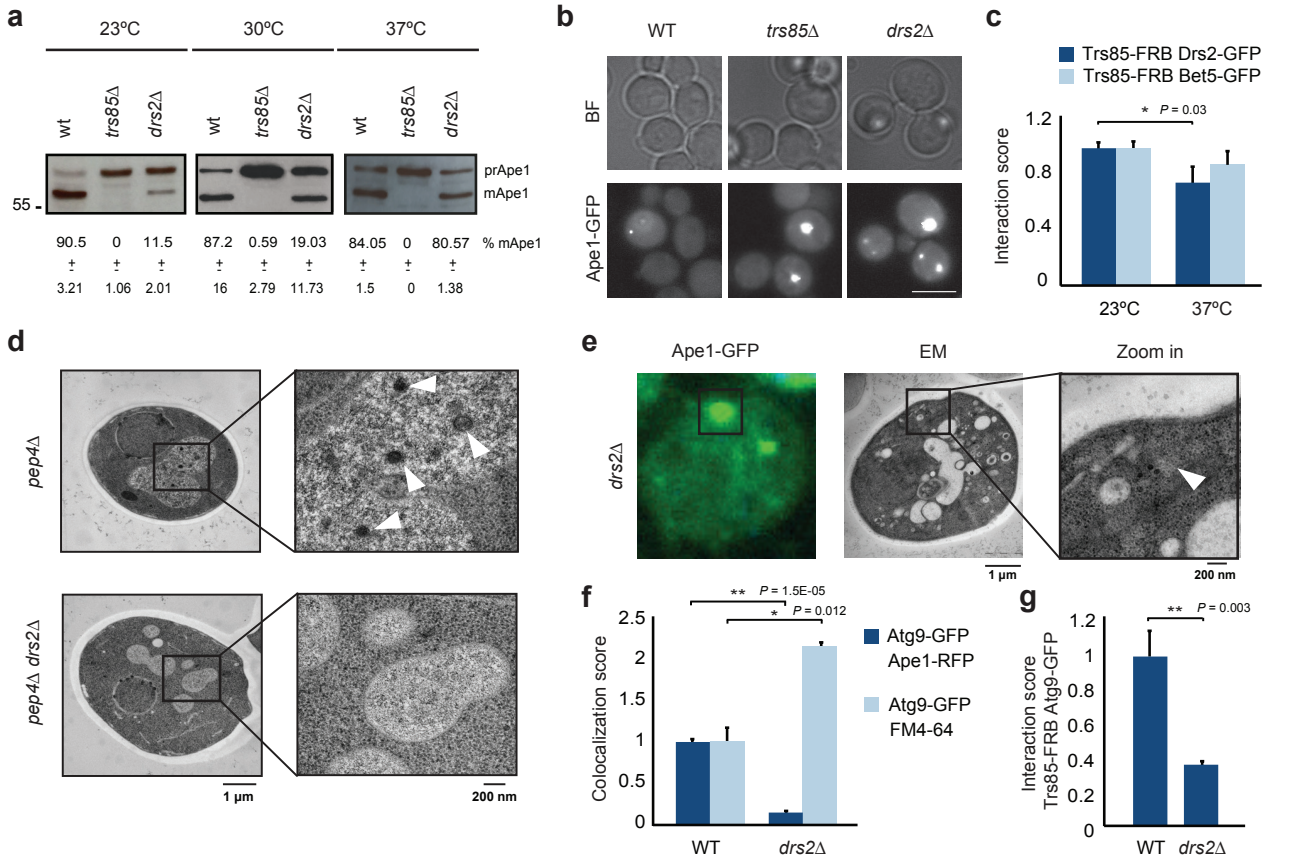

Fig. 2 Drs2 is critical for the biogenesis of the CVT vesicle at cold environments. **a** Processing of Ape1 was analyzed by western blot. Below, percentage of mApe1 ± SD. **b** Aggregation of prApe1. Representative images of Ape1-GFP in wild-type, *trs85*Δ and *drs2Δ* cells. BF, brightfield images. Scale bar, 5µm. **c** PICT assay for the interaction of Trs85-FRB (TRAPPIII) with Drs2-GFP or Bet5-GFP (TRAPIII). Interaction score was normalized to the measurement at 23ºC. **d** Representative EM images of *pep4Δ* and *pep4Δdrs2Δ* strains. Black squares show a zoom-in in the vacuole. White arrowheads point to CVT bodies. **e** Representative CLEM images of *drs2Δ* cells. Ape1-GFP (left) correlates with a membrane-free ribosome exclusion area (middle). Black square (right) shows a zoom-in at the position correlating with Ape1-GFP (white arrowhead). **f** Co-localization between Atg9-GFP and either Ape1-RFP or endocytic compartments stained with FM4-64 in wild-type and *drs2Δ* cells. Co-localization score was normalized to the corresponding wild-type cells. **g** PICT assay for the Trs85-FRB (TRAPPIII) and Atg9-GFP interaction. Interaction score was normalized to the measurement in wild-type cells. **a** and **c** Cells were grown at 30ºC until they reached log phase and then they were cultured at indicated temperatures for 2 hours. **b** and **d-g** Cells were grown at 30ºC until they reached log phase and then they were cultured at 23ºC for 2 hours before imaging. **a, c**, and **g** (Mean ± SD, $n = 3$) and **f** (Mean ± SD, $n \geq 2$). Asterisks indicate significant difference as determined by a two-tailed Student's t-test at **P < 0.01, and *P < 0.05, respectively).

In cells lacking TRAPPIII subunit Trs85 (*trs85*Δ), Atg9 is not delivered to the PAS, the biogenesis of the CVT vesicle is blocked and prApe1-GFP is accumulated in large cytosolic aggregates (Figs. 2a and 2b)[43,27].

Because Drs2 is essential for cell growth only at temperatures below 21ºC[44], we first analyzed the contribution of Drs2 in the CVT pathway at different temperatures. While *trs85*Δ cells cannot perform the CVT pathway in any of the temperatures tested, cells lacking Drs2 (*drs2*Δ) show a progressive inhibition of Ape1 maturation when decreasing the temperature. Thus, *drs2*Δ cells process prApe1 normally at 37°C but they can only mature 11.5% of the aminopeptidase when grown at 23°C (Fig. 2a). Consistently, cells lacking either Trs85 or Drs2 accumulate similar prApe1-GFP aggregates at the lower temperature (Fig. 2b and Supplementary Video 1). Indeed, Drs2-TRAPPIII binding is boosted in colder conditions: at 23ºC the Interaction score between Drs2 and Trs85 was 24% higher than at 37ºC (Fig. 2c), while no significant difference could be observed for the interaction of Trs85 and Bet5, another subunit of TRAPPIII. This observation suggests that the cell regulates the interplay between Drs2 and TRAPPIII in response to temperature shifts and thus provides Drs2 with additional functions in the CVT pathway at colder environments. Only traces of Ape1 processing could be detected in *drs2*Δ cells grown at 16ºC (Supplementary Fig. 1a). However, to avoid undesired effects derived from impairing cell viability, we continued studying the interplay between Drs2 and TRAPPIII at 23ºC.

We then used electron microscopy (EM) to study the ultrastructure of the CVT pathway. Pep4 is a protease required for the processing of the CVT vesicle once it is internalized in the vacuole[45]. While 89.3% of the *pep4*Δ cells presented CVT bodies inside the vacuole, we could not detect any CVT body-like structure in the vacuoles of *pep4*Δ*drs2*Δ cells (Fig. 2d). We then analyzed prApe1-GFP aggregates in *drs2*Δ cells with Correlative Light and Electron Microscopy (CLEM)[46]. 91.4% of the prApe1-GFP spots correlated with a ribosome exclusion area of amorphous shape and that was devoid of double membrane or CVT vesicle-like structure

(Fig. 2e). These results point to a critical role of Drs2 during the biogenesis of the CVT vesicle at 23ºC.

We used live-cell imaging to investigate TRAPPIII function in cells lacking Drs2. Atg9 delivered to the CVT vesicle by TRAPPIII can be tracked as the co-localization of Atg9-GFP and Ape1-RFP. In *drs2*Δ cells, the accumulation of Atg9-GFP at the Ape1-RFP aggregates was 79% lower than in wild-type cells. Instead, in *drs2*Δ cells the co-localization between Atg9-GFP and the FM4-64 dye staining the endosomal/vacuolar compartments increased more than 2-fold (Fig. 2f). This indicates that Drs2 is required for the correct delivery of Atg9 vesicles from endosomal/vacuolar compartments during the CVT pathway and that the TRAPPIII function relies on the presence of this flippase. Indeed, the deletion of Drs2 results in a 64% inhibition of the Interaction score between Trs85 and Atg9 (Fig. 2g). This residual binding between TRAPPIII and Atg9 goes in agreement with the observation that CVT pathway remains slightly active in *drs2*Δ cells grown at 23ºC (Fig. 2a). This was further demonstrated in cells lacking Drs2 and Atg19 (i.e. specific receptor for the CVT pathway), Drs2 and Atg17 (i.e. specific scaffold for non-selective autophagy) and in a time course assay (Supplementary Figs. 1b and 1c). Overall, these data suggest that at low temperatures, Drs2 and TRAPPIII form a functional module necessary for the correct delivery of Atg9 vesicles to the PAS and, subsequently, for the biogenesis of the CVT vesicle.

The role of Drs2 in CVT pathway is independent from its known mechanisms of action

We used yeast genetics to rule out the possibility that defects in the CVT pathway in *drs2*Δ cells result indirectly from the perturbation of other processes regulated by the flippase. Ape1 processing was not affected in cells lacking Rcy1 (i.e., cells where transport from early endosomes to TGN is blocked)[47,31], Apl4 (i.e., cells where the AP-1 pathway from TGN to early endosomes and the exit of the high-density class of vesicles from the TGN are blocked)[48,49], Apl5 (i.e., cells where ALP pathway from TGN to the vacuole is blocked)[50] or both Gga1 and Gga2 (i.e., cells where CPY pathway from TGN to late endosomes is blocked)[51] (Fig. 3a). Overall, genetic data suggest that the transport of Atg9 to the PAS involves a new function of Drs2 in the Drs2-TRAPPIII module.

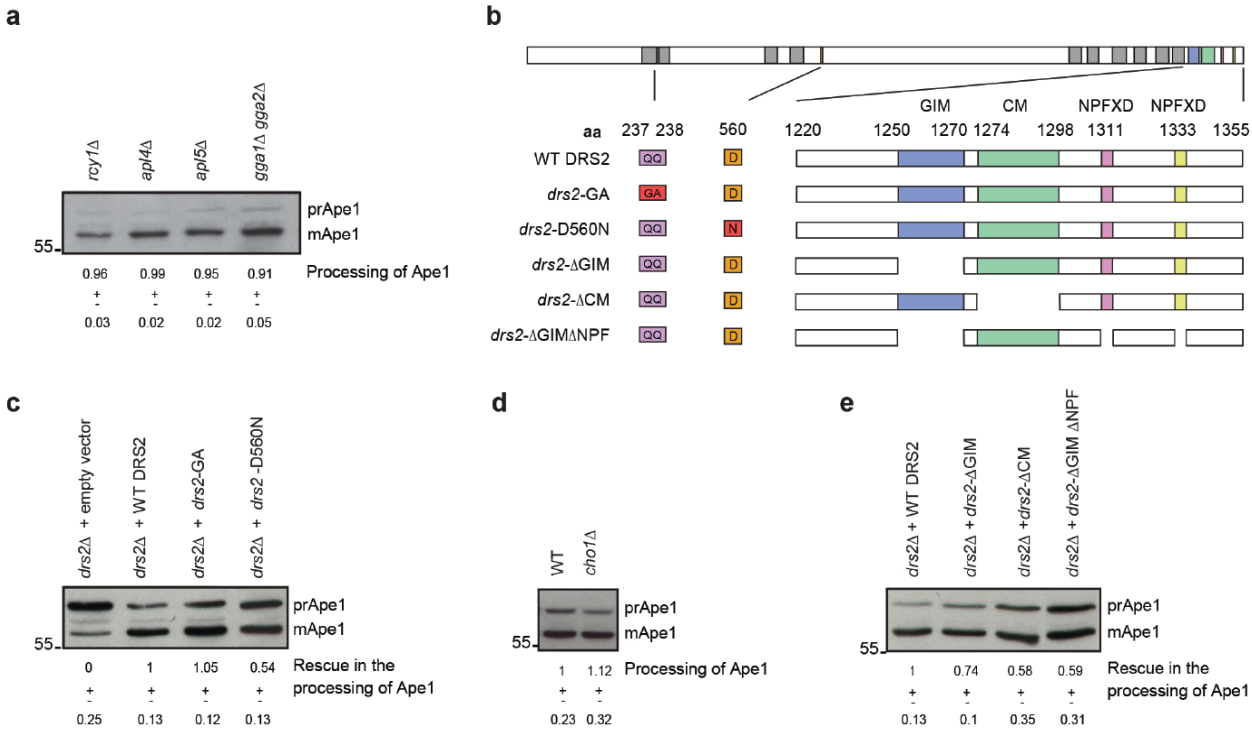

Fig. 3 Drs2 role in the CVT pathway is independent from its known mechanisms. **a** and **c-e** Processing of prApe1 was analyzed by western blot in the indicated strains. Cells were grown at 30ºC until they reached log phase and then they were cultured at 23ºC for 2 hours before analysis (n = 3). **a** Below, values of the percentage of matured Ape1 (mApe1) ± SD. **b** Representation of the main structural features of Drs2. Each color in the top bar indicates the location of a feature in the sequence of wild-type Drs2. Grey boxes depict transmembrane domains. Below, a summary of the mutants tested and an enlarged view of their C-terminal tail. QQ>GA and D>N mutations are depicted in red. Knock-out of a specific region is shown as an empty box. Numbers indicate the residues position in Drs2 sequence. **c** and **e** Cells harboring an empty plasmid and/or a plasmid coding for a wild-type Drs2 were used as control. Below, values of the mean rescue of Ape1 processing normalized to the rescue achieved in *drs2Δ* cells expressing wild-type Drs2 ± SD. **d** Below, values of percentage of matured Ape1 (mApe1) normalized to the percentage of mApe1 in wild-type cells ± SD.

We then explored the molecular mechanism of the Drs2-TRAPPIII module during the biogenesis of the CVT vesicle. We analyzed the rescue of Ape1 processing in *drs2*Δ cells that express different constructs of Drs2 (in all constructs Drs2 was expressed under the control of the DRS2 promoter) (Fig. 3b). We first targeted the PS flipping activity of Drs2, which is required for the bidirectional transport endosome-TGN and the exit of secretory vesicles from the TGN[52,53,54]. While cells harboring an empty vector do not rescue Ape1 processing in *drs2*Δ cells, cells expressing a mutant unable to flip PS (*drs2*-GA) and cells expressing an ATPase-dead mutant form of Drs2 (*drs2*-D560N) rescue the CVT pathway (Fig. 3c). Cells lacking Cho1, an enzyme essential for the synthesis of PS[55], show normal processing of Ape1, confirming that flipping of phospholipids is not involved in the mechanism of action of the Drs2-TRAPPIII module in the CVT pathway (Fig. 3d).

The cytosolic C-terminal tail is also important for the function of the Drs2. For instance, the Gea2 interacting motif (GIM) is required for the Drs2-Gea2-Arl1 complex assembly, a mechanism based on protein-protein interactions that regulate a number of trafficking pathways at the TGN and endosomes[56,57]. Adjacent to the GIM, Drs2 presents a conserved motif (CM). CM is fundamental for Drs2 function and to bind to the cytosolic domains that stabilize the autoinhibition of Drs2[57,40]. Drs2 has also two NPFXD motifs (hereafter referred to as NPF motif) that constitute some of its multiple endocytosis signals[58]. However, in agreement with yeast genetics, expression of *drs2*-ΔGIM, *drs2*-ΔCM or *drs2*-ΔGIMΔNPF rescued Ape1 processing (Fig. 3e). Thus, the mutagenesis experiments indicate that Drs2 C-terminal tail is not critical for the action of the Drs2-TRAPPIII module in the CVT pathway.

The I(S/R)TTK motif is required for the Drs2-TRAPPIII module and its function in the CVT pathway

We then investigated the cytosolic N-terminal tail of Drs2. Multiple sequence alignment identified a conserved stretch of 15 amino acids in the five P4-ATPases (residues 198-212 in Drs2; Fig. 4a). The stretch defines a cavity of 18.8 Å in depth located adjacent to the first transmembrane helix in the structure of Drs2 (Fig. 4b). Homology modeling of the other yeast P4-ATPases using Drs2 structure as template (PDB ID: 6ROH:A) suggests that the cavity is also conserved (Supplementary Fig. 2). However, only those P4-ATPases that bind MTCs present the I(S/R)TTK sequence at the bottom of the cavity. Thus, I(S/R)TTK is conserved in Drs2, Dnf1 and Dnf2 and it is absent in Dnf3 and Neo1. This correlation prompted us to investigate the contribution of this motif to the regulation of the Drs2-TRAPPIII module. We first generated cells

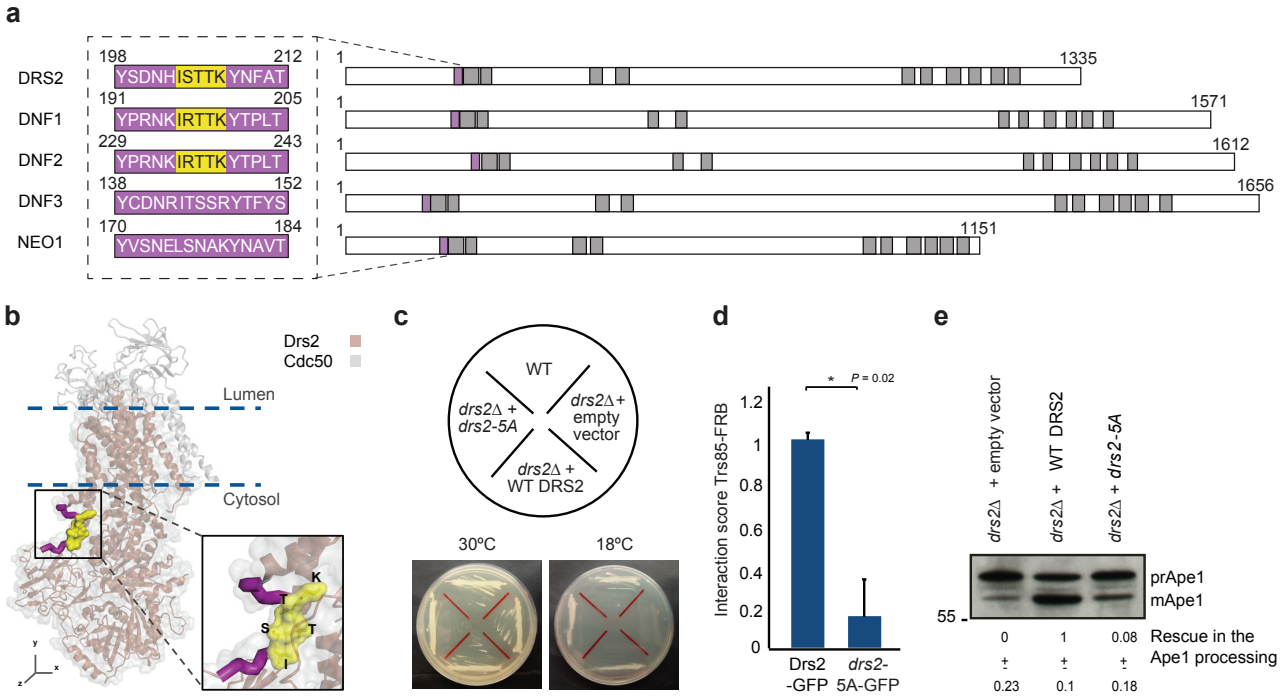

Fig. 4 The I(S/R)TTK motif is required for the assembly of the Drs2-TRAPPIII module and its function in the CVT pathway. **a** Representation of the 15 aa cavity (purple) in the N-terminal tail of P4-ATPases. Grey boxes depict transmembrane domains. Black dashed box shows the sequence coding for the cavity (left). Yellow background highlights the I(S/R)TTK motif in Drs2, Dnf1 and Dnf2. **b** The I(S/R)TTK motif in the Drs2-Cdc50 structure (PDB ID: 6ROH:A). Black box zooms in the cavity of Drs2 (purple) and the I(S/R)TTK motif (yellow). **c** Cold-sensitive assay for wild-type and *drs2Δ* cells expressing an empty vector, or plasmids coding for wild-type DRS2 or *drs2-5A* mutant. Cells streaked onto YPD plates were incubated at 30ºC and 18ºC for three days. **d** Interaction between TRAPPIII-FRB and Drs2-GFP or *drs2-5A*-GFP. The Interaction score was normalized to the measurement of the Drs2-GFP (Mean ± SD, $n = 2$. Asterisk indicates significant difference as determined by a two-tailed Student's t-test at $^*P < 0.05$). **e** Processing of Ape1. Cells were grown at 30ºC until they reached log phase and then they were cultured at 23ºC for 2 hours before analysis. Rescue of Ape1 processing was normalized to the rescue achieved in cells expressing wild-type Drs2 (Mean ± SD, $n = 3$).

expressing Drs2 with its I(S/R)TTK motif substituted by five alanines (*drs2*-5A). The expression of *drs2*-5A rescues the cold-sensitive phenotype of *drs2*Δ cells, confirming that the loss of this motif does not induce general protein unfolding (Fig. 4c). However, we could not detect the interaction between *drs2*-5A and Trs85 and the expression of *drs2*-5A in *drs2*Δ cells could not rescue Ape1 processing (Figs. 4d and 4e). Overall, these results indicate that the Drs2 I(S/R)TTK motif is required for the assembly of the Drs2-TRAPPIII module and its function in the CVT pathway.

Drs2 I(S/R)TTK mediates protein interactions central in the retrograde pathway

To systematically analyze the mechanism mediated by the Drs2 I(S/R)TTK motif, we performed crosslinking-mass spectrometry (XL-MS) immunoprecipitation experiments (see Methods). We used disuccinimidyl sulfoxide (DSSO), a crosslinker of 10.1Å in length that allowed us to detect proximal peptides in cell extracts[59]. Upon a GFP-specific pulldown, the comparative analysis between the interactome of Drs2-GFP and *drs2*-5A-GFP identified 26 proteins whose interaction is diminished by the mutation of the I(S/R)TTK motif (Fig. 5). This set of interactions is enriched with proteins involved in endosomal transport (*P*=3.9 E-06), Golgi vesicle transport (*P*=3.5 E-05) and endosome-to-Golgi transport (*P*=4.9 E-08). This includes the retromer subcomplex Vps5/Vps17 and the Sec1p/Munc-18 protein Vps45, components of the machinery that regulates the late-endosome-to-Golgi transport together with GARP[60,61]. On the other side, known protein-protein interactions required for Drs2 function were not affected (e.g., binding to Cdc50 or Rcy1). Thus, in agreement with the cold-sensitivity rescue assay (Fig. 4c), the interactome data suggest that the mutation of the I(S/R)TTK motif allows us to dissect different mechanisms controlled by Drs2.

Consistent with our prediction that the I(S/R)TTK motif regulates the network of interactions between P4-ATPases and MTCs, *drs2*-5A-GFP could not recapitulate the interaction with Trs65, Trs120 and Trs130 (specific subunits of TRAPPII), Trs85 (the specific subunit of TRAPPIII) and Vps53 (GARP) (Fig. 5). All TRAPPII, TRAPPIII and GARP complexes have been shown to contribute to the transport of Atg9[27,24]. Indeed, the interactions affected by the lost of the I(S/R)TTK motif include six proteins that bind Atg9: Trs85, Vps45, Pep1, Vps17, Vti1 and Akr1, the last two being components of the Atg9 vesicles[10] (Fig. 5). Overall, our results underscore the relevance of the I(S/R)TTK motif to mediate the interaction with the machinery controlling the distribution of Atg9 between the endocytic compartments and the Golgi, and suggest that Drs2 function involves additional mechanisms beyond the action of the Drs2-TRAPPIII module.

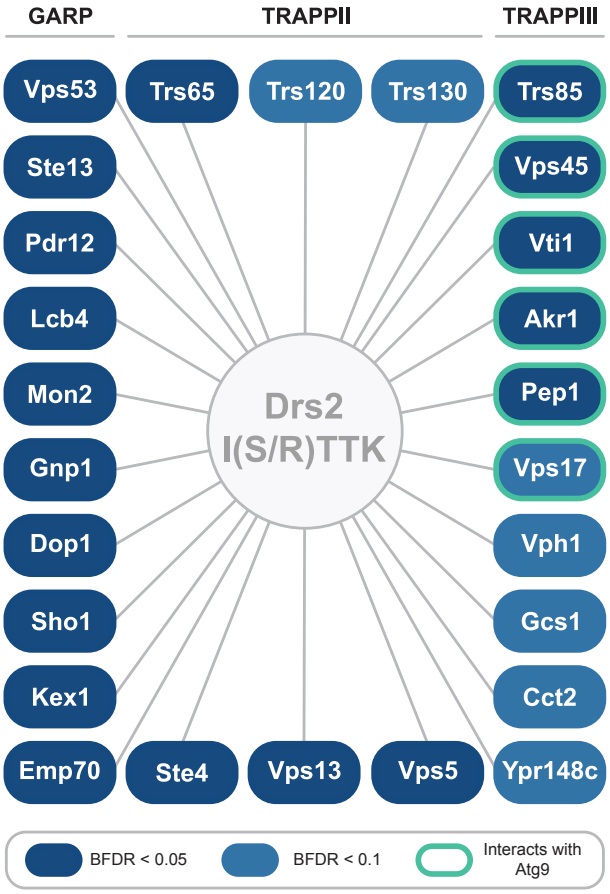

Fig. 5 Graphic representation of the 26 proteins whose interaction with Drs2 is diminished by the mutation of the I(S/R)TTK motif. BFDR, Bayesian False Discovery Rate.

Drs2 I(S/R)TTK is fundamental for Atg9 homeostasis

In growing yeast cells, Atg9-GFP can be observed as highly mobile puncta, the vast majority of which correspond to vesicles within the cytoplasm[11]. We implemented a microscopy-based system with high-sensitivity and high-temporal resolution to investigate the role of Drs2 in the trafficking Atg9 vesicles (see Methods). In agreement with other publications[11], growing wild-type cells present two populations of Atg9 puncta (Fig. 6a and Supplementary Video 2). The larger population comprises 86% of the puncta and it is highly mobile (mean speed of 2.3 ± 0.7 nm/ms). The smaller population comprises 14% of the puncta and it has slower mobility (mean speed of 0.7 ± 0.2 nm/ms). In cells lacking TRAPPIII, there is a 2-fold increase in the slower population of Atg9 puncta (27% and a mean speed of 0.8 ± 0.3 nm/ms) (Fig. 6a and Supplementary Video 3). Interestingly, in *drs2*Δ and *drs2*-5A cells, the low mobility population increases up to 54% (0.6 ± 0.3 nm/ms) and 50% (0.6 ± 0.2 nm/ms), respectively (Fig. 6a and Supplementary Videos 4 and 5). Thus, vesicle tracking demonstrates that, at low temperature, the I(S/R)TTK motif of Drs2 plays a major role in the trafficking of Atg9 vesicles. Importantly, the relevance of Drs2 to maintain the homeostasis of Atg9 cannot be accounted for its role in the Drs2-TRAPPIII module

only. Thus, function of Drs2 in the transport of Atg9 is likely to involve the interaction with other components of the membrane traffic machinery. We could not detect Drs2-GFP at the PAS (Supplementary Fig. 1d), supporting the hypothesis that Drs2 regulates Atg9 homeostasis at the crossroad between endosomes and Golgi, where it can bind TRAPPII, TRAPPIII and GARP.

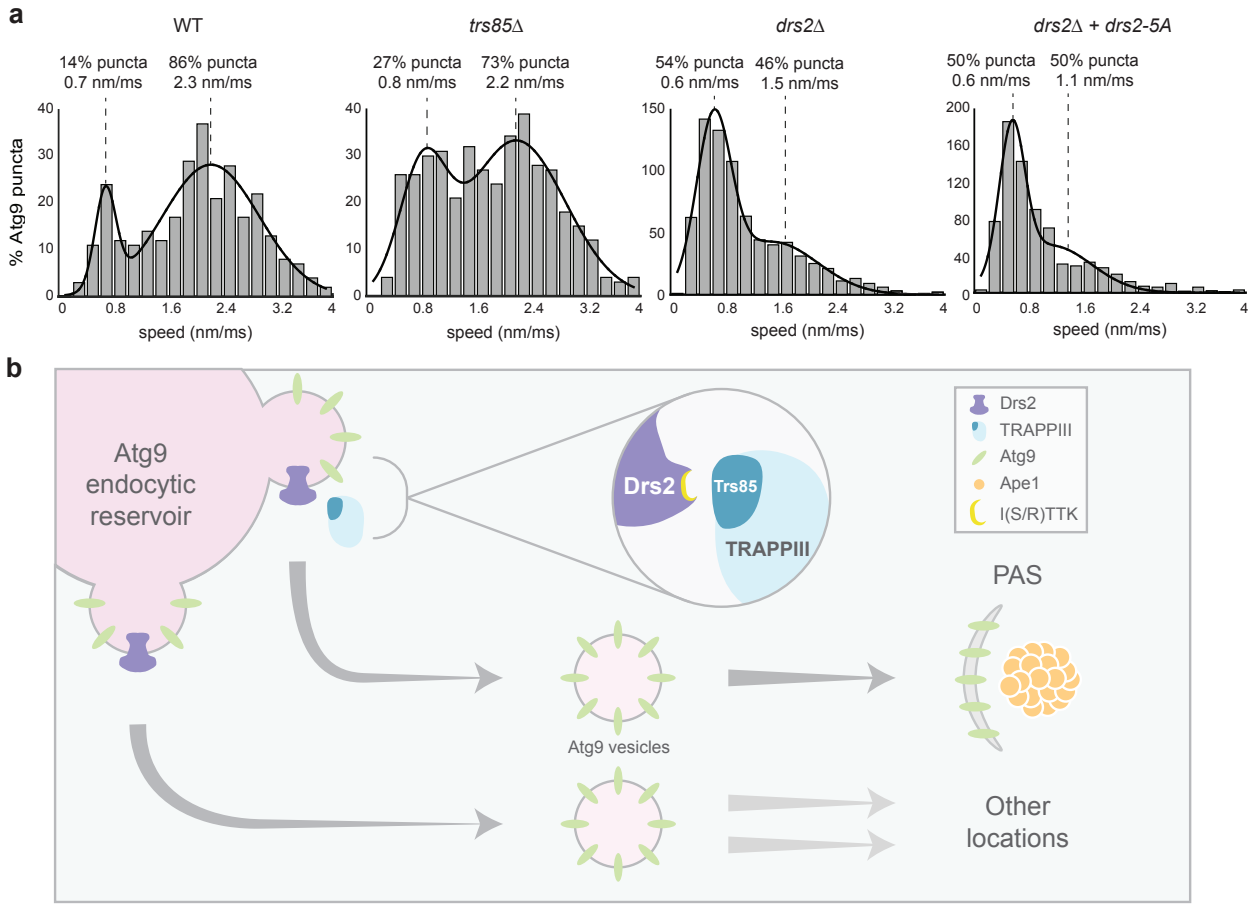

Fig. 6 I(S/R)TTK motif of Drs2 plays a central role in the transport of Atg9. **a** Histograms representing the mean speed of Atg9 puncta observed in wild-type, *trs85Δ, drs2Δ* cells and *drs2-5A* cells. The histograms were fitted to a mixture of Gaussian distributions with two components; medians of the fitting curves and percentage of each population are indicated on top of the plot. **b** Model for the regulation of Atg9 vesicles by the I(S/R)TTK motif of Drs2. Drs2 through its I(S/R)TTK motif forms a functional module with TRAPPIII required for the circulation of Atg9 vesicles to the PAS during selective autophagy. The I(S/R)TTK motif of Drs2 is also required for the exit of Atg9 vesicles from their reservoirs in the endocytic pathway and that are targeted to other locations in the cell.

Discussion

Understanding the mode of action of MTCs requires a comparative analysis of the mechanistic features that are common in these protein machines. Genetic interactions and a more sensitive PICT assay allowed us to systematically explore transient and low abundant binding events relevant to MTCs function[29]. We found that MTCs localizing at the Golgi form a network of protein-protein interactions with P4-ATPases. Whether these interactions are required for the onset of vesicle transport or the delivery of the vesicle to the acceptor membrane could not be anticipated. We used Drs2 to study the relevance and the mechanistic features of the interplay between MTCs and P4-ATPases in the transport of Atg9.

The majority of the Atg9 circulates between reservoirs at the endocytic structures and the Golgi. However, a small fraction is delivered to the PAS, where it is required for the biogenesis of CVT vesicles[27] (Fig. 6b). We reasoned that the Drs2-TRAPPIII module is likely not involved in the tethering of Atg9 vesicles in selective autophagy because we could not detect Drs2-GFP in the PAS (Supplementary Fig. 1d). Instead, co-localization and vesicle tracking experiments indicate that Drs2 is critical for the onset of Atg9 vesicles from the endocytic reservoirs, probably at early endosomes where both Drs2 and TRAPPIII play critical roles[27,31,62]. The distribution of Atg9 is adjusted dynamically to fulfill the cell needs under different circumstances. For instance, in exponentially growing cells, TRAPPIII is essential for transporting Atg9 from early endosomes, while the function of this complex is bypassed by the GARP in starved cells[27]. Our analysis of the CVT pathway demonstrated that in response to temperature shifts, the cell also modulates the assembly of the Drs2-TRAPPIII module to preserve an optimal Atg9 distribution. Combining

genetic interactions, live-cell imaging and ultrastructure analysis, we found that colder environments endow the Drs2-TRAPPIII module with an essential role in the transport of Atg9 to the PAS and the biogenesis of the CVT vesicle (Fig. 6b). A former study showing that *drs2*Δ cells process prApe1 normally at the stationary phase would suggest that Drs2 function is also modulated by the cellular growth[26].

This work provides insight into the mechanism that regulates the assembly of the Drs2-TRAPPIII module. Drs2 controls several trafficking pathways at endosomes and the Golgi by flipping PS and nesting protein-protein interactions at the C-terminal domain[53,31,54]. However, genetic experiments showed that the function of Drs2 in the biogenesis of the CVT vesicle is independent of these mechanisms and it does not rely on previously reported functions of the flippase in vesicle trafficking. Instead, binding to TRAPPIII and efficient Ape1 processing relies on the I(S/R)TTK motif nested at the bottom of the cavity of Drs2 N-terminal tail, linking the first transmembrane helix and the actuator domain[40].

The cavity is conserved in the atomic structure of yeast and human P4-ATPases[40,41,63,64,65]. The presence of the I(S/R)TTK motif in yeast Dnf1 and Dnf2 and the related ISTAK motif in the human ATP8A2, a homolog of Drs2, suggests a conserved mechanism for the interplay with MTCs (Supplementary Figs. 2 and 3). The structural analysis of human ATP8A1 showed that the cavity is transiently unfolded in the transition between the E2P and E2Pi-PL states along the lipid translocation cycle. During this rearrangement, the neck of the cavity switches from a close conformation of 14.1Å to an open conformation of 20.6Å (Cys50-to-Asn60)[63]. This suggests that the Drs2 cavity might undergo similar conformational dynamics during the assembly of the Drs2-TRAPPIII module, which would expose the I(S/R)TTK motif.

To gain mechanistic insight about the Drs2 I(S/R)TTK motif, we used mutagenesis and XL-MS with DSSO (spacer length of 10.1 Å)[59] to explore the interactome that is in close proximity to Drs2. We could not detect binding of Drs2-GFP to any subunit of the COG complex, suggesting that Drs2 and COG do not interact in close proximity at low temperatures. However, we confirmed that the Drs2 I(S/R)TTK motif is required for the binding to GARP, TRAPPII and TRAPPIII. For the last two, the mutation of the Drs2 I(S/R)TTK motif exclusively hampers binding to their specific subunits. This is consistent with a mechanism where both TRAPP complexes recognize the flippase through their specific subunits.

XL-MS also provided information about the mode of action of Drs2 to control the transport of Atg9. We uncovered interactions between Drs2 and proteins regulating vesicle trafficking in endosomes and the Golgi. In addition to the TRAPPIII specific subunit Trs85, Drs2 I(S/R)TTK motif mediates the interaction with five proteins that bind Atg9: Vps17, Akr1, Vti1, Pep1 and Vps45. Accordingly, mutations of TRAPPIII caused a significant yet limited impact in the mobility of Atg9 (15% decrease of the highly mobile fraction of Atg9 puncta), while the mutation of Drs2 I(S/R)TTK motif resulted in a larger reduction of the Atg9 mobility (42% decrease of the highly mobile fraction of Atg9 puncta) (Fig. 6a). These results show that the contribution of Drs2 in the transport of Atg9 is not limited to the pathway controlled by TRAPPIII, but it could also involve other MTCs such as TRAPPII and GARP. This is further supported by recent discovery of Drs2 localization in Atg9 vesicles[10] and the enrichment of DRS2 genetic interactions with genes coding for proteins involved in autophagy ($P = 0.002$).

MTCs, which are fundamental to sustain vesicle transport in any eukaryotic cell, base their mechanism of action on protein-protein interactions with other components of the trafficking machinery, such as GTPases and SNAREs. In this study, we have identified a network of interactions with P4-ATPases that involve key proteins for the biogenesis of vesicles at the endosomes and the Golgi. To our knowledge, MTCs and P4-ATPases have never been described to interact or to act in concert during vesicle transport[39,66,67,68]. We have investigated the mechanistic details that control the interplay between Drs2 and TRAPPIII in the transport of Atg9 and have uncovered a pathway required for selective autophagy at low temperatures. The role of TRAPPIII in other pathways, such as the secretory pathway, underscores the need to perform further studies to characterize the role of the Drs2-TRAPPIII module in the transport of COPII vesicles. Although the mechanism inducing the activation of the Drs2-TRAPPIII module in cold temperatures remains unknown, our data indicate that the network between MTCs and P4-ATPases is subjected to critical regulation in response to environmental cues. Thus, the interplay between other MTCs and P4-ATPases might be induced under conditions yet to be explored.

Methods

Yeast strains, plasmids and cultures

Saccharomyces cerevisiae strains are derivatives of BY4741 or BY4742 backgrounds. Strains with genes coding for C-terminal tags, deleted genes, and/or mutated alleles were generated by homologous recombination following standard PCR strategies[69]. Those strains harboring exogenous genes coded in plasmids were generated by transformation. All Drs2 constructs were expressed from a plasmid using the DRS2 promoter. All strains are listed in Supplementary Tables 1-4. All plasmids used are listed in Supplementary Table 5.

Strains used for the PICT assay express the anchor Tub4-RFP-FKBP and harbor different combinations of baits (FRB fusions) and preys (GFP fusions at the C-terminus) (see Supplementary Tables 1, 2, 3)[29]. Parental cells expressing the anchor Tub4-RFP-FKBP and a bait-FRB were constructed on the OGY0307 genetic background. Parental cells expressing the prey-GFP were constructed in the BY4741 genetic background or obtained from the genomic C-terminal GFP fusion collection (ThermoFisher). Excluding those strains harboring plasmids that code for Drs2-GFP and *drs2*-5A-GFP, the PICT experiments were done with yeast strains constructed with the SGA approach[70].

Yeast cells were grown in YPD liquid medium at 30ºC and 220 rpm until saturation (≈16h). Cells harboring plasmids were grown in synthetic minimal liquid medium lacking the amino acid of choice. In experiments with *cho1Δ* cells, the medium was supplemented with 1mM Ethanolamine. After, cells were diluted to an optical density of OD_{600}=0.2 in the medium of interest and cultured at 30ºC and 220 rpm until they reached an early logarithmic phase (OD_{600}≈1). Unless indicated, cells were then incubated at 23ºC for two hours before performing the experiment.

Imaging

After saturation in the YPD culture, cells were diluted and grown in Low Flo medium (Yeast Nitrogen Base Low Fluorescence without Amino acids, Folic Acid and Riboflavin, 2% Synthetic complete Mixture Dropout (lacking essential amino acids as required) and 2% glucose). When they reached an early logarithmic phase (OD_{600}≈1), cells were either imaged (experiments Fig. 1) or further grown to the desired temperature and time (experiments Fig. 2-6 and Supplementary Fig. 1). Before imaging, cells were attached to Concanavalin A (0.1µg/mL)-coated glass bottom plates. When required, 10µM of rapamycin were added 20-30 minutes before imaging. Images were acquired on an ScanR (Olympus) microscope based on a IX81 stand, equipped with 100x/1.40 objective lens, an Orca-ER camera (Hamamatsu), a MT20 Xenon arc lamp illumination system holding excitation filter and two complete fluorescence filter cubes from AHF respectively optimized for GFP (ET Bandpass 470/40 + Beamsplitter 500 DVXRUV + ET Bandpass 525/50) and RFP (ET Bandpass 545/30 + Beamsplitter 580 DVXRUV + BrightLine HC 617/73). For the experiments shown in Fig. 1, automated imaging acquisition was carried out. The acquisition software (ScanR, Olympus) was set up to detect those cells' planes with the highest RFP signal. This provided a focal plane that captured the highest number of anchoring platforms in focus. Images were obtained sequentially by switching the filter cubes. Strains were imaged in the RFP (200ms) and GFP channels (200 and 1500ms in Fig. 1a and 1b; 200 and 1000ms in Fig. 1d) and each strain was imaged in at least 6 fields of view. In one-to-one experiments (Fig. 2c, 2g and 4d), cells were imaged using Xcellence (Olympus) as acquisition software. Strains were imaged in the RFP (200ms) and the GFP (exposition time was optimized manually) channels.

Protein interactions from Imaging Complexes after Translocation (PICT)

PICT technique allows the quantitative characterization of protein-protein interactions *in vivo*. The addition of rapamycin to culture media induces FRB-FKBP heterodimerization and translocation of the protein tagged to FRB (bait-FRB) to anchoring platforms engineered in the cell by tagging an anchoring molecule to RFP and FKBP (Anchor-RFP-FKBP). GFP-tagged proteins (prey-GFP) that are bound to the bait-FRB are co-translocated to these anchoring platforms. These changes in localization can be subsequently quantified using dual-color live-cell imaging. Recently, we increased PICT sensitivity up to 200-fold. We designed a new anchoring platform by tagging Tub4, a component of the spindle pole body, with RFP and FKBP (Tub4-RFP-FKBP). The resulting cells harbor one or two anchoring platforms only. Thus, even low abundant complexes accumulate enough prey-GFP in each of these anchoring platforms to be efficiently detected and quantified[29]. All PICT experiments were performed in rapamycin-insensitive strains carrying the *tor*1-1 mutation in the TOR1 gene and where the endogenous FPR1 gene was deleted[28]. Images were taken prior and after rapamycin addition.

Selection of proteins for the protein-protein interaction screen

First we identified the bait-FRBs of each MTC that allows anchoring more efficiently the fully assembled complex (Fig. 1a and Supplementary Table 2). For each MTC we generated a set of strains expressing all possible combinations of subunits tagged to FRB and GFP. Then, we selected the corresponding bait-FRB that showed highest Interaction score for the other subunit of the corresponding complex.

Then we used genetic interactions to select the prey-GFPs for the screen. *S. cerevisiae* has 8 MTC complexes, each of them with a different protein composition. Genes coding for MTC subunits (MTC Gene or GM) interact genetically with 1283 genes (Candidate Genes or CG) in yeast (SGD September 2013). In total, *S. cerevisiae* has 5820 genes.

For each Candidate and MTC Gene pair CG_i-GM_j, we calculated its pairwise interaction probability P_{ij} given by:

$P_{ij} = PC_{ij} * PM_{ji}$

where PC_{ij} is the probability that a Candidate Gene *i* interacts with MTC Gene *j*; and PM_{ji} is the probability that MTC Gene *j* interacts with Candidate Gene *i*.

When a Candidate Gene *i* interacts genetically with a set *J* of subunits of a given MTC, we use a genetic score S_i defined as

$$S_i = \prod_{j \in J} P_{ij}$$

to measure the probability of measuring randomly the genetic interaction profile with Candidate Gene *i*.

676 Candidate Genes with a "Genetic interaction score" < 10^{-6} were selected for further analysis. We then selected the corresponding 470 prey proteins that are included in the yeast C-terminally GFP-tagged genomic collection[71] and whose binding to MTC subunits had not been described (Supplementary Table 1).

Image analysis

A custom image analysis workflow was implemented as an ImageJ (http://rsb.info.nih.gov/ij/) macro to automate operations and process whole data sets. Essentially, this workflow aimed to estimate the co-

localization (overlap) between spots independently segmented in the images from RFP (anchors) and GFP (preys) channels.

To exclude out of focus (or empty) images, a sharpness factor was first computed (standard deviation of the image intensity normalized to its mean intensity in RFP channel). The fields of view with sharpness factor above a user defined threshold were processed by the following sequence of operations aiming to segment bright spots: 1) smoothening, 2) background subtraction, 3) local thresholding, 4) median filtering and 5) discard small particles below a certain area. For each experimental condition, the functional parameters of the workflow were manually optimized to lead to the best results.

The area of overlap between preys and anchors was then estimated by counting the number of foreground pixels common in both segmentation masks (logical AND operation). This area was then normalized to the count of foreground pixels in the RFP segmentation mask (anchors area) to lead to the *fractional anchor to prey overlap* $\boldsymbol{F_o}$. Next, the mean intensity $\boldsymbol{I_o}$ from the GFP channel was estimated inside the regions of spot overlap and the weighted average of $\boldsymbol{F_o}$. $\boldsymbol{I_o}$ was computed over the whole field of view (anchors area used for weighting).

Analysis of PICT experiments

In the primary selection of positive hits (screening of Fig. 1b), a Fold change was estimated for each condition as the ratio between the weighted average of $\boldsymbol{F_o}$. $\boldsymbol{I_o}$ after and prior to rapamycin addition (see Fold change values in Supplementary Table 1). An arbitrary Fold change of 3 was established as potential interactions. This primary list was manually curated and confirmed in one-to-one PICT experiments.

We defined an Interaction score as the subtraction of the weighted average of $\boldsymbol{F_o}$. $\boldsymbol{I_o}$ prior to rapamycin addition from the weighted average of $\boldsymbol{F_o}$. $\boldsymbol{I_o}$ upon rapamycin addition. In PICT experiments conducted to determine the most efficient baits used to anchor each MTC (Fig. 1a and Supplementary Table 2) and to evaluate the network of interactions between P4-ATPases and MTCs (Fig. 1d and Supplementary Table 3), an arbitrary Interaction score of 100 was established to identify positive interactions. This primary list was manually validated. All one-to-one PICT experiments (Fig. 2c, 2g and 4d) were done in at least two biological replicates. For the statistical analysis, the Interaction score of one-to-one experiments was normalized to the measurement of those strains expressing wild-type Drs2 (Fig. 2g and 4d) or to the measurement of those strains after two hours at 23ºC (Fig. 2c).

Co-localization assays

Similar as described above, the co-localization score $\boldsymbol{S_o}$ was determined as the area of overlap between GFP and RFP channels estimated by counting the number of foreground pixels common in both segmentation masks (logical AND operation) over all fields of view (GFP area used for weighting) (Fig. 2f). For the statistical analysis, the co-localization score was estimated in cells harboring wild-type or deleted DRS2 and normalized to the measurement of those strains expressing wild-type Drs2. Co-localization experiments in Fig. 2f were done in at least two biological replicates.

In Fig. 2f and Supplementary Video 1, cells grown in YPD were labelled with 8µM FM4-64. Prior to imaging, cells were kept in the dark for 10 or 30 minutes to stain endocytic structures or the vacuole, respectively. Then cells were washed twice with Low Flo liquid medium to remove YPD and free FM4-64 before imaging. Imaris software was used to obtain the 3D reconstruction of yeast cells imaged with Z-stacks of 250nm step in size (Supplementary Video 1).

Vesicle tracking

The protocol used for the tracking of Atg9 vesicles is based on the method reported previously[11]. Atg9 was C-terminally fused to a 3xGFP tag. The best focal plane was selected for imaging and 2D time-lapses were acquired at 20 frames per second with a 488 nm laser excitation providing a power of approximately 50mW at the back aperture of the objective lens, placed on an inverted microscope (IX71 Olympus) optimized for oblique illumination and fast acquisition (Hamamatsu Flash4 v2 sCMOS camera) with a 100x/1.45 objective lens. Oblique illumination reduces background signal and the high-speed camera allows high-temporal resolution. The axial extension of the laser inclined sheet was approximately 1.5 to 2µm and the usable field of view approximately 40x40µm; images were cropped to increase acquisition speed and illumination was kept continuous during the time-lapses. More than 290 trajectories of GFP puncta were collected from several time-lapses for each strain.

The images were compensated for bleaching by applying the correction method “Exponential fit” from ImageJ “Bleach Correction” plugin. Individual vesicles were then identified and tracked by ImageJ TrackMate plugin[72]. The tracks were linked with “simple LAP” option, a maximal linking distance of 5 pixels and no gap-closing allowed. Finally, only tracks containing a minimum of 5 spots were kept to discard spurious tracks.

For each time-lapse, the average speed of the vesicles was computed within tracks and binned to a 20 bin histogram spanning from 0 to 200 nm/frame. The resulting histograms were fitted to a two-component Gaussian mixture model (GMM). The fits were optimized by the nonlinear least-squares regression (MATLAB). From these models, we estimated the mean speed (and standard deviation) for both populations. The fraction of spots belonging to each population was derived as the fractional areas below each Gaussian component normalized to the area below the fitted curve.

Electron microscopy (EM) and Correlative Light and Electron microscopy (CLEM)

Cells were grown as described before. High-pressure freezing, freeze-substitution and embedding in EM and CLEM experiments were performed as described in the literature[73]. In brief, yeast cells were pelleted and the yeast paste was loaded into 200µm depth planchettes and high-pressure frozen using the High Pressure Freezing Leica EM ICE. The planchette sandwich was disassembled under liquid nitrogen prior to freeze-substitution. Samples were freeze-substituted using a temperature-controlling AFS2 (Leica) with an FPS robot.

EM pictures were then taken at various magnifications in a JEOL JEM 1011 electron microscope equipped with a Veleta 2k x 2k side-mounted TEM CCD camera (Olympus).

For CLEM experiments, samples were stored protected from light after polymerization and processed further within two days. Ultrathin sections were cut with a diamond knife in a microtome (Leica EM UC7) and picked up on carbon-coated 200 mesh copper grids. Fluorescent fiducial markers, 0.02µm Blue FluoSpheres (Molecular Probes) (excitation 365 nm/emission 415nm) were adhered to the section. Then grids were placed section-face down onto a 15µl drop of FluoSpheres for 10 min, blotted with filter paper and washed with three drops of water with blotting between the washing steps. To minimize bleaching, fluorescence images were taken with an IX83 (Olympus) during the next three days. From 2 to 5 images were taken in different focal planes for both channels (GFP and blue fluorescent fiducials). During imaging, the positions on the grid of the imaged areas of interest were recorded. EM pictures of recorded positions were taken and correlated to the corresponding GFP images. We detected Ape1-GFP aggregates in 2% of the cells of our sections (n=660).

Immunoblot analysis

Cells were grown as described before. An alkaline extraction method described in Kushnirov, V, 2000[74] was followed to prepare the samples for western blot analysis. The blocking step was done with 5% milk powder in TBS-0.5% Tween 20 for one hour at room temperature. Incubation with primary anti-Ape1 antibody was done overnight at 4ºC (1:4000 antibody dilution in blocking solution). Incubation with secondary anti-rabbit antibody was done for one hour at room temperature (1:2500 antibody dilution in blocking solution).

Western Blot quantification was done with the ImageStudio™Lite software. In the exported data, the background of the prApe1 and mApe1 bands' signal intensities is automatically corrected from a region right under or above the band. To calculate the % mApe1, the signal intensity of mApe1 multiplied by its band area was divided by the result of the addition of the signal intensities of prApe1 and mApe1, each one multiplied by its corresponding band area.

Cross-linking and immunoprecipitation

Cells were grown as described before. 600 OD_{600} units of yeast cells were washed twice with B88 buffer (19.97mM HEPES pH=6.8, 149.77mM KOAc, 250.32mM sorbitol, 4mM MgOAc). Cell lysis was performed using Freezer/Mill® Cryogenic Grinder (Spex®SamplePrep, model 6775). Cell powder was resuspended in 5ml B88 + PMSF + protein inhibitor and centrifuged to eliminate cell debris. The supernatant was taken and DSSO was added to a final concentration of 2.5mM. After 20 minutes, 0.5M glycine was added to stop the reaction. The mix was incubated for 5min. Triton X-100 was added to a final concentration of 1%. The suspension was incubated with rotation for 1h at 4ºC before removing the insoluble components by 13000rpm centrifugation at 4ºC during 1h. For the immunoprecipitation, the samples were incubated for 1 h with previously equilibrated Bab agarose beads (Chromotek) at 4ºC. Then, they were incubated with GFP-Trap_Agarose (Chromotek) overnight at 4ºC. The resin was first washed 4 times with a solution containing 8M urea, 2M NaCl and 1% TX-100 in PBS, and it was subsequently washed 4 more times with PBS.

The resin used in immunoprecipitation was cleaned three times with 500µl of 200mM ammonium bicarbonate and 60µl of 6M urea/200mM ammonium bicarbonate were added. Samples were then reduced with dithiothreitol (30nmol, 37ºC, 60 min), alkylated in the dark with iodoacetamide (60nmol, 25ºC, 30 min) and diluted to 1M urea with 200mM ammonium bicarbonate for trypsin digestion (1µg, 37ºC, 8 h, Promega cat # V5113).

After digestion, peptide mix was acidified with formic acid and desalted with a MicroSpin C18 column (The Nest Group, Inc) prior to LC-MS/MS analysis.

Chromatographic and mass spectrometric analysis

Samples were analyzed using a LTQ-Orbitrap Velos Pro mass spectrometer (Thermo Fisher Scientific, San Jose, CA, USA) coupled to an EASY-nLC 1000 (Thermo Fisher Scientific (Proxeon), Odense, Denmark). Peptides were loaded onto the 2-cm Nano Trap column with an inner diameter of 100µm packed with C18 particles of 5µm particle size (Thermo Fisher Scientific) and were separated by reversed-phase chromatography using a 25-cm column with an inner diameter of 75µm, packed with 1.9µm C18 particles (Nikkyo Technos Co., Ltd. Japan). Chromatographic gradients started at 93% buffer A and 7% buffer B with a flow rate of 250nl/min for 5 minutes and gradually increased 65% buffer A and 35% buffer B in 60 min. After each analysis, the column was washed for 15 min with 10% buffer A and 90% buffer B. Buffer A: 0.1% formic acid in water. Buffer B: 0.1% formic acid in acetonitrile.

The mass spectrometer was operated in positive ionization mode with nanospray voltage set at 2.1 kV and source temperature at 300°C. Ultramark 1621 for the was used for external calibration of the FT mass analyzer prior the analyses, and an internal calibration was performed using the background polysiloxane ion signal at m/z 445.1200. The acquisition

was performed in data-dependent acquisition (DDA) mode and full MS scans with 1 micro scans at resolution of 60,000 were used over a mass range of m/z 350-2000 with detection in the Orbitrap. Auto gain control (AGC) was set to 1E6, dynamic exclusion (60 seconds) and charge state filtering disqualifying singly charged peptides was activated. In each cycle of DDA analysis, following each survey scan, the top twenty most intense ions with multiple charged ions above a threshold ion count of 5000 were selected for fragmentation. Fragment ion spectra were produced via collision-induced dissociation (CID) at normalized collision energy of 35% and they were acquired in the ion trap mass analyzer. AGC was set to 1E4, isolation window of 2.0 m/z, an activation time of 10 ms and a maximum injection time of 100 ms were used. All data were acquired with Xcalibur software v2.2.

Digested bovine serum albumin (New england biolabs cat # P8108S) was analyzed between each sample to avoid sample carryover and to assure stability of the instrument and QCloud[75] has been used to control instrument longitudinal performance during the project.

Mass spectrometric data Analysis

Acquired spectra were analyzed using the Proteome Discoverer software suite (v1.4, Thermo Fisher Scientific) and the Mascot search engine (v2.6, Matrix Science)[76]. The data were searched against a *S. cerevisiae* Genome database (as in November 2019, 6080 entries) plus a list[77] of common contaminants and all the corresponding decoy entries. For peptide identification, a precursor ion mass tolerance of 7 ppm was used for MS1 level, trypsin was chosen as enzyme and up to three missed cleavages were allowed. The fragment ion mass tolerance was set to 0.5 Da for MS2 spectra. Oxidation of methionine and N-terminal protein acetylation were used as variable modifications whereas carbamidomethylation on cysteines was set as a fixed modification. False discovery rate (FDR) in peptide identification was set to a maximum of 5%. PSM were normalized by the median of Drs2 PSM.

SAINTexpress algorithm was used to score protein-protein interactions[78].

Structural modeling

Protein flippases Dnf1, Dnf2, Dnf3 and Neo1 were modelled by using Modeller from the HHSearch server[79], using Drs2 as a template (PDB ID: 6ROH:A). The ATP8A2 homology model was obtained with Modeller from the HHSearch server[79], using ATP8A1 as template (PDB ID: 6K7N). Images were generated using PyMOL[80].

Gene Ontology enrichment analysis

The p-value (*P*) for the Gene Ontology enrichment was calculated using the Hypergeometric distribution corrected by the Bonferroni method of multiple test correction.

Data availability

Data supporting the findings of this manuscript are available from the corresponding authors upon reasonable request. The raw proteomics data will be deposited to the PRIDE[81] repository once the manuscript is accepted for publication.

References

1. Baba, M., Takeshige, K., Baba, N. & Ohsumi, Y. Ultrastructural analysis of the autophagic process in yeast: Detection of autophagosomes and their characterization. *J. Cell Biol.* **124**, 903–913 (1994).
2. Baba, M., Osumi, M. & Ohsumi, Y. Analysis of the Membrane Structures Involved in Autophagy in Yeast by Freeze-Replica Method. *Cell Struct. Funct.* **20**, 465–471 (1995).
3. Kanki, T. & Klionsky, D. J. Mitophagy in yeast occurs through a selective mechanism. *J. Biol. Chem.* **283**, 32386–32393 (2008).
4. Krick, R. *et al.* Piecemeal Microautophagy of the Nucleus Requires the Core Macroautophagy Genes. *Mol. Biol. Cell.* **19**, 4492–4505 (2008).
5. Scott, S. V. *et al.* Cytoplasm-to-vacuole targeting and autophagy employ the same machinery to deliver proteins to the yeast vacuole. *Proc. Natl. Acad. Sci. U. S. A.* **93**, 12304–12308 (1996).
6. Lynch-Day, M. A. & Klionsky, D. J. The Cvt pathway as a model for selective autophagy. *FEBS Lett.* **584**, 1359–1366 (2010).
7. Gatica, D., Lahiri, V. & Klionsky, D. J. Cargo recognition and degradation by selective autophagy. *Nat. Cell Biol.* **20**, 233–242 (2018).
8. Wilfling, F. *et al.* A Selective Autophagy Pathway for Phase-Separated Endocytic Protein Deposits. *Mol. Cell.* **80**, 764-778.e7 (2020).
9. Matoba, K. *et al.* Atg9 is a lipid scramblase that mediates autophagosomal membrane expansion. *Nat. Struct. Mol. Biol.* **27**, 1185–1193 (2020).
10. Sawa-Makarska, J. *et al.* Reconstitution of autophagosome nucleation defines Atg9 vesicles as seeds for membrane formation. *Science.* **369**, eaaz7714 (2020).
11. Yamamoto, H. *et al.* Atg9 vesicles are an important membrane source during early steps of autophagosome formation. *J. Cell Biol.* **198**, 219–233 (2012).
12. Yu, I.-M. & Hughson, F. M. Tethering factors as organizers of intracellular vesicular traffic. *Annu Rev Cell Dev Biol.* **26**, 137–156 (2010).
13. Bröcker, C., Engelbrecht-Vandré, S. & Ungermann, C. Multisubunit tethering complexes and their role in membrane fusion. *Curr. Biol.* **20**, 943–952 (2010).
14. Suvorova, E. S., Duden, R. & Lupashin, V. V. The Sec34/Sec35p complex, a Ypt1p effector required for retrograde intra-Golgi trafficking, interacts with Golgi SNAREs and COPI vesicle coat proteins. *J. Cell Biol.* **157**, 631–643 (2002).
15. Ren, Y. *et al.* A Structure-Based Mechanism for Vesicle Capture by the Multisubunit Tethering Complex Dsl1. *Cell.* **139**, 1119–1129 (2009).
16. Balderhaar, H. J. k. & Ungermann, C. CORVET and HOPS tethering complexes - coordinators of endosome and lysosome fusion. *J. Cell Sci.* **126**, 1307–1316 (2013).
17. Elizabeth Conibear, Jessica N. Cleck, and T. H. S. Vps51p Mediates the

Association of the GARP (Vps52/ 53/54) Complex with the Late Golgi t-SNARE Tlg1p. *Mol. Biol. Cell*. **21**, 1610–1623 (2002).

18. Heider, M. R. *et al.* Subunit connectivity, assembly determinants, and architecture of the yeast exocyst complex. *Nat Struct Mol Biol.* **23**, 59–66 (2016).
19. Yu, S. & Liang, Y. A trapper keeper for TRAPP, its structures and functions. *Cell. Mol. Life Sci.* **69**, 3933–3944 (2012).
20. Thomas, L. L., Joiner, A. M. N. & Fromme, J. C. The TRAPPIII complex activates the GTPase Ypt1 (Rab1) in the secretory pathway. *J. Cell Biol.* **217**, 283–298 (2018).
21. Yip, C. K., Berscheminski, J. & Walz, T. Molecular architecture of the TRAPPII complex and implications for vesicle tethering. *Nat. Struct. Mol. Biol.* **17**, 1298–1304 (2010).
22. Tan, D. *et al.* The EM structure of the TRAPPIII complex leads to the identification of a requirement for COPII vesicles on the macroautophagy pathway. *Proc. Natl. Acad. Sci. U. S. A.* **110**, 19432–19437 (2013).
23. Morozova, N. *et al.* TRAPPII subunits are required for the specificity switch of a Ypt-Rab GEF. *Nat. Cell Biol.* **8**, 1263–1269 (2006).
24. Zou, S. *et al.* Trs130 participates in autophagy through GTPases Ypt31/32 in Saccharomyces cerevisiae. *Traffic.* **14**, 233–246 (2013).
25. Reggiori, F., Wang, C. W., Stromhaug, P. E., Shintani, T. & Klionsky, D. J. Vps51 is part of the yeast Vps fifty-three tethering complex essential for retrograde traffic from the early endosome and Cvt vesicle completion. *J. Biol. Chem.* **278**, 5009–5020 (2003).
26. Wang, I. H., Chen, Y. J., Hsu, J. W. & Lee, F. J. S. The Arl3 and Arl1 GTPases co-operate with Cog8 to regulate selective autophagy via Atg9 trafficking. *Traffic.* **18**, 580–589 (2017).
27. Shirahama-Noda, K., Kira, S., Yoshimori, T. & Noda, T. TRAPPIII is responsible for vesicular transport from early endosomes to Golgi, facilitating Atg9 cycling in autophagy. *J. Cell Sci.* **126**, 4963–4973 (2013).
28. Gallego, O. *et al.* Detection and Characterization of Protein Interactions In Vivo by a Simple Live-Cell Imaging Method. *PLoS One.* **8**, 1–6 (2013).
29. Torreira, E. *et al. The dynamic assembly of distinct RNA polymerase i complexes modulates rDNA transcription*. *eLife.* **6**, (2017).
30. Natarajan, P., Wang, J., Hua, Z. & Graham, T. R. Drs2p-coupled aminophospholipid translocase activity in yeast Golgi membranes and relationship to in vivo function. *Proc. Natl. Acad. Sci. U. S. A.* **101**, 10614–10619 (2004).
31. Hanamatsu, H., Fujimura-Kamada, K., Yamamoto, T., Furuta, N. & Tanaka, K. Interaction of the phospholipid flippase Drs2p with the F-box protein Rcy1p plays an important role in early endosome to trans-Golgi network vesicle transport in yeast. *J. Biochem.* **155**, 51–62 (2014).
32. Michael Costanzo, Baryshnikova, A., L Myers, C., Andrews, B. & Boone, C. Charting the genetic interaction map of a cell. *Curr. Opin. Biotechnol.* **22**, 66–74 (2011).
33. Chen, J., Zheng, X. F., Brown, E. J. & Schreiber, S. L. Identification of an 11-kDa FKBP12-rapamycin-binding domain within the 289-kDa FKBP12-rapamycin-associated protein and characterization of a critical serine residue. *Proc. Natl. Acad. Sci. U. S. A.* **92**, 4947–4951 (1995).
34. Protopopov, V., Govindan, B., Novick, P. & Gerst, J. E. Homologs of the synaptobrevin/VAMP family of synaptic vesicle proteins function on the late secretory pathway in S. cerevisiae. *Cell.* **74**, 855–861 (1993).
35. Balderhaar, H. J. K. *et al.* The CORVET complex promotes tethering and fusion of Rab5/Vps21-positive membranes. *Proc. Natl. Acad. Sci. U. S. A.* **110**, 3823–3828 (2013).
36. Zhou, F. *et al.* A Rab5 GTPase module is important for autophagosome clouser. *PLoS Genet.* **13**, 1–24 (2017).
37. Saito, K. *et al.* Cdc50p, a protein required for polarized growth, associates with the Drs2p P-type ATPase implicated in phospholipid translocation in Saccharomyces cerevisiae. *Mol. Biol. Cell.* **15**, 3418–3432 (2004).
38. Sebastian, T. T., D, B. R., Xu, P. & Graham, T. R. Phospholipid flippases: building asymmetric membranes and transport vesicles. *Biochim Biophys Acta.* **1821**, 1068–1077 (2012).
39. Hua, Z., Fatheddin, P. & Graham, T. R. An Essential Subfamily of Drs2p-related P-Type ATPases Is Required for Protein Trafficking between Golgi Complex and Endosomal/Vacuolar System. *Mol. Biol. Cell.* **13**, 3162–3177 (2002).
40. Timcenko, M. *et al.* Structure and autoregulation of a P4-ATPase lipid flippase. *Nature.* **571**, 366–370 (2019).
41. Bai, L. *et al.* Autoinhibition and activation mechanisms of the eukaryotic lipid flippase Drs2p-Cdc50p. *Nat. Commun.* **10**, 1–10 (2019).
42. Guimaraes, R. S., Delorme-Axford, E., Klionsky, D. J. & Reggiori, F. Assays for the biochemical and ultrastructural measurement of selective and nonselective types of autophagy in the yeast Saccharomyces cerevisiae. *Methods.* **75**, 141–150 (2015).
43. Meiling-Wesse, K. *et al.* Trs85 (Gsg1), a component of the TRAPP complexes, is required for the organization of the preautophagosomal structure during selective autophagy via the Cvt pathway. *J. Biol. Chem.* **280**, 33669–33678 (2005).
44. Chen, C.-Y., Ingram, M. F., Rosal, P. H. & Graham, T. R. Role for Drs2p, a P-Type ATPase and Potential Aminophospholipid Translocase, in Yeast Late Golgi Function. *J Cell Biol.* **147**, 1223–1236 (1999).
45. Baba, M., Osumi, M., Scott, S. V., Klionsky, D. J. & Ohsumi, Y. Two distinct pathways for targeting proteins from the cytoplasm to the vacuole/lysosome. *J. Cell Biol.* **139**, 1687–1695 (1997).
46. Kukulski, W. *et al.* Correlated fluorescence and 3D electron microscopy with high sensitivity and spatial precision. *J. Cell Biol.* **192**, 111–119 (2011).
47. Furuta, N., Fujimura-Kamada, K., Saito, K., Yamamoto, T. & Tanaka, K. Endocytic Recycling in Yeast Is Regulated by Putative Phospholipid Translocases and the Ypt31p/32p–Rcy1p Pathway. *Mol. Biol. Cell.* **18**, 295–312 (2007).
48. Liu, K., Surendhran, K., Nothwehr, S. F. & Graham, T. R. P4-ATPase Requirement for AP-1/Clathrin Function in Protein Transport from the trans-Golgi Network and Early Endosomes. *Mol. Biol. Cell.* **19**, 3526–3535 (2008).
49. Hinners, I. Changing directions: clathrin-mediated transport between the Golgi and endosomes. *J. Cell Sci.* **116**, 763–771 (2003).
50. Odorizzi, G., Cowles, C. R. & Emr, S. D. The AP-3 complex: a coat of many colours. *Trends Cell Biol.* **8**, 282–288 (1998).
51. Sakane, H., Yamamoto, T. & Tanaka, K. The functional relationship between the Cdc50p-Drs2p putative aminophospholipid translocase and the Arf GAP Gcs1p in vesicle formation in the retrieval pathway from yeast early endosomes to the TGN. *Cell Struct. Funct.* **31**, 87–108 (2006).
52. Xu, P., Baldridge, R. D., Chi, R. J., Burd, C. G. & Graham, T. R.

Phosphatidylserine flipping enhances membrane curvature and negative charge required for vesicular transport. *J. Cell Biol.* **202**, 875–886 (2013).

53. Liu, K., Surendhran, K., Nothwehr, S. F. & Graham, T. R. P4-ATPase Requirement for AP-1/Clathrin Function in Protein Transport from the trans-Golgi Network and Early Endosomes. *Mol. Biol. Cell.* **19**, 3526–3535 (2008).
54. Alder-Baerens, N., Lisman, Q., Luong, L., Pomorski, T. & C.M, H. J. Loss of P4 ATPases Drs2p and Dnf3p Disrupts Aminophospholipid Transport and Asymmetry in Yeast Post-Golgi Secretory Vesicles. *Mol. Biol. Cell.* **17**, 1632–1642 (2006).
55. Choi, H. S., Han, G. S. & Carman, G. M. Phosphorylation of yeast phosphatidylserine synthase by protein kinase A: Identification of SER46 and SER47 as major sites of phosphorylation. *J. Biol. Chem.* **285**, 11526–11536 (2010).
56. Tsai, P.-C., Hsu, J.-W., Liu, Y.-W., Chen, K.-Y. & Lee, F.-J. S. Arl1p regulates spatial membrane organization at the trans-Golgi network through interaction with Arf-GEF Gea2p and flippase Drs2p. *Proc. Natl. Acad. Sci. U. S. A.* **110**, E668–E677 (2013).
57. Chantalat, S. The Arf activator Gea2p and the P-type ATPase Drs2p interact at the Golgi in Saccharomyces cerevisiae. *J. Cell Sci.* **117**, 711–722 (2004).
58. Liu, K., Hua, Z., Nepute, J. A. & Graham, T. R. Yeast P4-ATPases Drs2p and Dnf1p Are Essential Cargos of the NPFXD/Sla1p Endocytic Pathway. *Mol. Biol. Cell.* **18**, 487–500 (2007).
59. Kao, A. *et al.* Development of a Novel Cross-linking Strategy for Fast and Accurate Identification of Cross-linked Peptides of Protein Complexes. *Mol. Cell. Proteomics* **10**, M110.002212 (2011).
60. Dulubova, I. *et al.* How Tlg2p/syntaxin 16 'snares' Vps45. *EMBO J.* **21**, 3620–3631 (2002).
61. Eising, S., Thiele, L. & Fröhlich, F. A systematic approach to identify recycling endocytic cargo depending on the GARP complex. *Elife.* **8**, 1–22 (2019).
62. Furuta, N., Fujimura-Kamada, K., Saito, K., Yamamoto, T. & Tanaka, K. Endocytic recycling in yeast is regulated by putative phospholipid translocases and the Ypt31p/32p-Rcy1p pathway. *Mol Biol Cell.* **18**, 295–312 (2007).
63. Hiraizumi, M., Yamashita, K., Nishizawa, T. & Nureki, O. Cryo-EM structures capture the transport cycle of the P4-ATPase flippase. *Science.* **365**, 1149–1155 (2019).
64. Nakanishi, H. *et al.* Transport Cycle of Plasma Membrane Flippase ATP11C by Cryo-EM. *Cell Rep.* **32**, 108208 (2020).
65. Nakanishi, H. *et al.* Crystal structure of a human plasma membrane phospholipid flippase. *J. Biol. Chem.* **295**, 10180–10194 (2020).
66. Gall, W. E. *et al.* Drs2p-dependent formation of exocytic clathrin-coated vesicles in vivo. *Curr. Biol.* **12**, 1623–1627 (2002).
67. Lee, S. *et al.* Transport through recycling endosomes requires EHD1 recruitment by a phosphatidylserine translocase. *EMBO J.* **34**, 669–688 (2015).
68. Roland, B. P. & Graham, T. R. Decoding P4-ATPase Substrate Interactions. *Crit Rev Biochem Mol Biol.* **51**, 513–527 (2016).
69. Janke, C. *et al.* A versatile toolbox for PCR-based tagging of yeast genes: New fluorescent proteins, more markers and promoter substitution cassettes. *Yeast.* **21**, 947–962 (2004).
70. Tong, Y. & Boone, C. Synthetic Genetic Array Analysis in Saccharomyces cerevisiae. *Methods Mol. Biol.* **313**, 171–192 (2005).
71. Huh *et al.* Global analysis of protein localization in budding yeast. *Nature* .**425**, 686–691 (2003).
72. Tinevez, J. Y. *et al.* TrackMate: An open and extensible platform for single-particle tracking. *Methods.* **115**, 80–90 (2017).
73. Müller-Reichert, M. *Correlative Light and Electron Microscopy*. (2012).
74. Kushnirov, V. V. Rapid and reliable protein extraction from yeast. *Yeast.* **16**, 857–860 (2000).
75. Chiva, C. *et al.* QCloud: A cloud-based quality control system for mass spectrometry-based proteomics laboratories. *PLoS One.* **13**, 1–14 (2018).
76. Perkins, D. N., Pappin, D. J., Creasy, D. M. & Cottrell, J. S. Probability-based protein identification by searching sequence databases using mass spectrometry data. *Electrophoresis.* **20**, 3551–3567 (1999).
77. Beer, L. A., Liu, P., Ky, B., Barnhart, K. T. & Speicher, D. W. Efficient quantitative comparisons of plasma proteomes using label-free analysis with MaxQuant. *Methods Mol Biol*. **1619**, 339–352 (2017).
78. Guoci Teo *et al.* SAINTexpress: improvements and additional features in Significance Analysis of Interactome software. *J Proteomics.* **100**, 37–43 (2014).
79. Zimmermann, L. *et al.* A Completely Reimplemented MPI Bioinformatics Toolkit with a New HHpred Server at its Core. *J. Mol. Biol.* **430**, 2237–2243 (2018).
80. The PyMOL Molecular Graphics System, Version 2.3.4 Schrödinger, LLC.
81. Vizcaíno, J. A. *et al.* 2016 update of the PRIDE database and its related tools. *Nucleic Acids Res.* **44**, D447–D456 (2016).

Acknowledgements

The proteomics analyses were performed in the CRG/UPF Proteomics Unit which is part of the of Proteored, PRB3 and is supported by grant PT17/0019, of the PE I+D+i 2013-2016, funded by ISCIII and ERDF. We thank Josep Vilardell, Bernat Crosas, Amy Curwin, Vivek Malhotra, Michael Knop, Marko Kaksonen, Kenji Maeda and Charles Boone for providing devices, reagents, strains and plasmids. We thank the Advanced Digital Microscopy Core Facility (ADMCF), the Biostatistics/Bioinformatics and the Mass Spectrometry and Proteomics facilities of the IRB Barcelona for live-cell imaging, technical support and also sharing devices with us. We thank Simona Barankova and Radovan Dojcilovic for fruitful discussions. We thank Raúl Méndez and Ignasi Fita for their support and mentoring during these years. OG was funded by research grants from the Spanish funding agency (MINECO; BFU2012-36385, PGC2018-095745-B-I00 and EUR2019-103815) and supported by the "Unidad de Excelencia María de Maeztu", funded by the MINECO (ref: MDM-2014-0370). IP was supported by FPI awarded by the Spanish Ministry of Economy and Competitiveness (MINECO) (ref: BES-2013-063945) and EMBO Short-Term Fellowship 7076.

Author contribution

I.P., T.G., M.M., M.H. and O.G. designed the research; I.P., A.C., A.G., A.N., C.B., E.A., J.C., M.A., M.P, N.J., S.T. and O.G. conducted the experiments and performed the analysis; and O.G. and I.P. discussed results and wrote the manuscript.

Competing interests

The authors declare no competing interests.

Additional information

Supplementary Information accompanies this paper at:

Correspondence and requests for materials should be addressed to O.G.
Email: oriol.gallego@upf.edu